Diagnostics of Accelerating Plasma

4th Semi-Annual Progress Report

Sept. 1, 1967 - Feb. 29, 1968

Report No. 68-005

DEPARTMENT OF SPACE SCIENCE & APPLIED PHYSICS

The Catholic University of America
Washington, D.C. 20017

NATIONAL AERONAUTICS AND SPACE ADMINISTRATION

Research Grant NGR-09-005-025

Diagnostics of Accelerating Plasma

4th Semi-Annual Progress Report

Sept. 1, 1967 - Feb. 29, 1968

Report No. 68-005

by

T.N. Lie , K.F. Lee

and

C.C. Chang

March 1 1968

Department of Space Science and Applied Physics
The Catholic University of America
Washington, D.C.

Abstract

The current-sheet velocities in two groups of coaxial plasma accelerators, one using refractory and the other non-refractory materials as insulators, are compared. There exists a large difference in sheet velocity between the two groups of accelerators in all cases, i.e., the velocities in the accelerators with non-refractory insulators are slower than the others. A direct cause for this is the marked difference between the two groups of accelerators in the radial current carried by the current sheet. The impurity mass flow which follows the current-sheet is observed particularly with the non-refractory insulator. The experimental results obtained here generally support the physical model on insulator ablation originally proposed by Keck. The accelerators with refractory insulators and with clean system also have a similar process and the sheet velocity is limited. In this case, however, degassing of light gas, e.g. hydrogen from the insulator wall, is probably responsible for the drag rather than ablation. An analysis of the ablation problem is made, mainly following Workman's results with the inclusion of an additional dimensionless parameter. The comparison between the analysis and measurements shows reasonable agreement over a wide area of accelerator operation.

TABLE OF CONTENT

LIST OF ILLUSTRATION

I. Introduction

The propagation velocity of the current-sheet in a coaxial plasma accelerator is, in general, limited (i.e., the velocity does not increase beyond a certain value even if the total energy input to the accelerator is drastically increased). This may be one of the causes of the discrepancy observed between theory and experiment. The velocity limitations of the current-sheet in a coaxial plasma accelerator have been studied by a number of investigators previously. Thom, Norwood and Jalufka [1] suggested that a drag force associated with ions striking the cathode acts on the accelerating plasma. The velocity drag depends on the ion-electron partition in the current-sheet and also on the atomic weight of the ambient gas used. This drag is very high with the heavier gases such as argon or air but is negligibly small with lighter gases [2] and this does not account for the velocity limitation generally observed in various species of gas. There exists some possibility of a drag due to the growth of a viscous boundary layer on the electrode wall behind the current-sheet. But, again the viscous drag is considered to be too small [2] to provide an explanation of the limiting velocity. Keck [2] suggested that the velocity limitation observed in his magnetic annular shock tube may be due to insulator ablation. Noting that only a portion of the total discharge current appears to move down the accelerator in the current-sheet, he has concluded that part of the drive current is trapped near the insulator end wall. The ionized vapor of ablated material near the insulator wall provides the current path and the additional mass introduced by the vapor contributes as an inertial drag.

This problem has been taken up in this laboratory because we felt that this kind of drag may be one of the major loss mechanism in the coaxial plasma accelerator and that it is

1

far greater than the drag due to the inertia of the ambient gas itself. Keck's physical model on the wall ablation was examined experimentally and existing analysis on the problem was generalized to make it fit with the experimental result obtained. It is found that the insulator wall ablation is indeed a serious velocity drag not only in an accelerator where non-refractory materials are used as insulators but also with refractory insulators such as vycor or quartz which provide a similar loss to the sheet propagation. The insulators of the latter-type material degass (presumably hydrogen) rather than ablate themselves and again act as a strong drag at a higher velocity of the current-sheet. Furthermore, dirtier accelerator with a refractory insulator is found to behave more or less the same manner as accelerator with a non-refractory insulator.

II. Velocity Limitation due to Insulator Ablation

A. Accelerators and Experimental Arrangement

The dimensions of the coaxial plasma accelerators used in this investigation are listed in Table I with their schematic diagram. The three accelerators used differ only in the inner electrode diameters – the outer electrode diameter is kept the same. The length of the electrodes is 22 cm. Two slots, $\frac{1}{32}$" wide and 15 cm long, are provided on the outer electrode along the accelerator axis for the optical measurement. The insulator which spearates the two cylindrical electrodes at the accelerator breech has the shape of a flat circular disc with a hole at the center. The insulating materials used so far are lucite, mylar, alumina, pyrex and vycor glass and these are easily interchanged by removing the inner electrode. The accelerator electrodes are enclosed by a vacuum chamber 9-inch in diameter and 60 inches long which is made of plexiglass. A capacitor of 60 µF capacity is charged up to 10 KV and the discharge is initiated by triggering a vacuum spark switch [3]. The quarter cycle time of the discharge is about 3.5 µsec, which is rather slow compared with our previous investigations. Maximum discharge current with 10 KV charging voltage is about 160 KA. The accelerator is operated with static filling of the gases rather than a injection of propellant gas. The working gases used are hydrogen, helium, nitrogen, and argon in the pressure range of 0.03 to 1.5 torr. The base pressure of the vacuum chamber prior to the gas filling is always below 1 milli-torr, and after each shot the chamber is pumped down and the gas is refilled to insure the purity of the gas. In addition to this, a cold trap is used in the vacuum system to minimize the back flow of the diffusion pump oil.

3

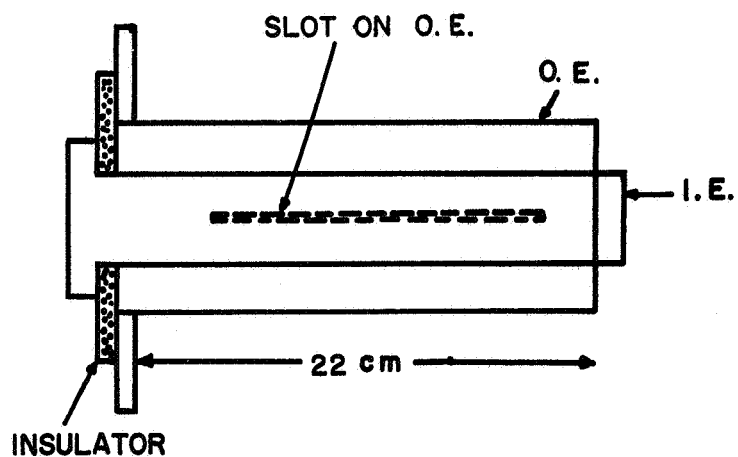| ACCELERATOR	DIA. OF O.E. (mm)	DIA. OF I.E. (mm)	INSULATOR
# 7 A	60	22	VYCOR, MYLER, PYREX, LUCITE
# 7 B	60	32	PYREX, LUCITE
# 7 C	60	40	LUCITE

Table I   Dimensions of Coaxial Plasma Accelerator

Most of the experimental measurements in the investigation consist of accurate determination of the luminous front velocity. This is done by taking streak photographs through the slot in the outer electrode of the moving plasma. An image converter camera with a streak unit is used for the photography. Since the velocity of the luminous front varies with time at the beginning of the quarter cycle as the discharge current increases, the velocity measurements are made at a fixed phase or a fixed time of the discharge cycle rather than made at fixed position of the accelerator barrel. This is done by recording oscillograms of the discharge current and the image converter streak monitoring signal from the camera simultaneously. Fig. 1 shows a typical streak photograph and the oscillograms of the discharge current and the streak signal recorded simultaneously. As can be seen, the luminous front is usually well defined for the gas pressure range used in this investigation and the shot-to-shot reproducibility of the measurement is 10 per cent or better in most cases. One notices bright second fronts in the photograph which have approximately the same velocity as first front. As already reported in previous reports [4,5], the first and second front in the streak photograph correspond to the portions of current-sheet which intersect with the inner and the outer electrodes, respectively. The second front is usually brighter than the first front because this part of the current-sheet, along the outer electrode wall, forms a well-defined ring where the electron density is rather high.

B. Velocity Difference

Although Keck proposed a possibility of drag due to the insulator ablation, a systematic check on the sheet velocity difference between the accelerators with refractory and
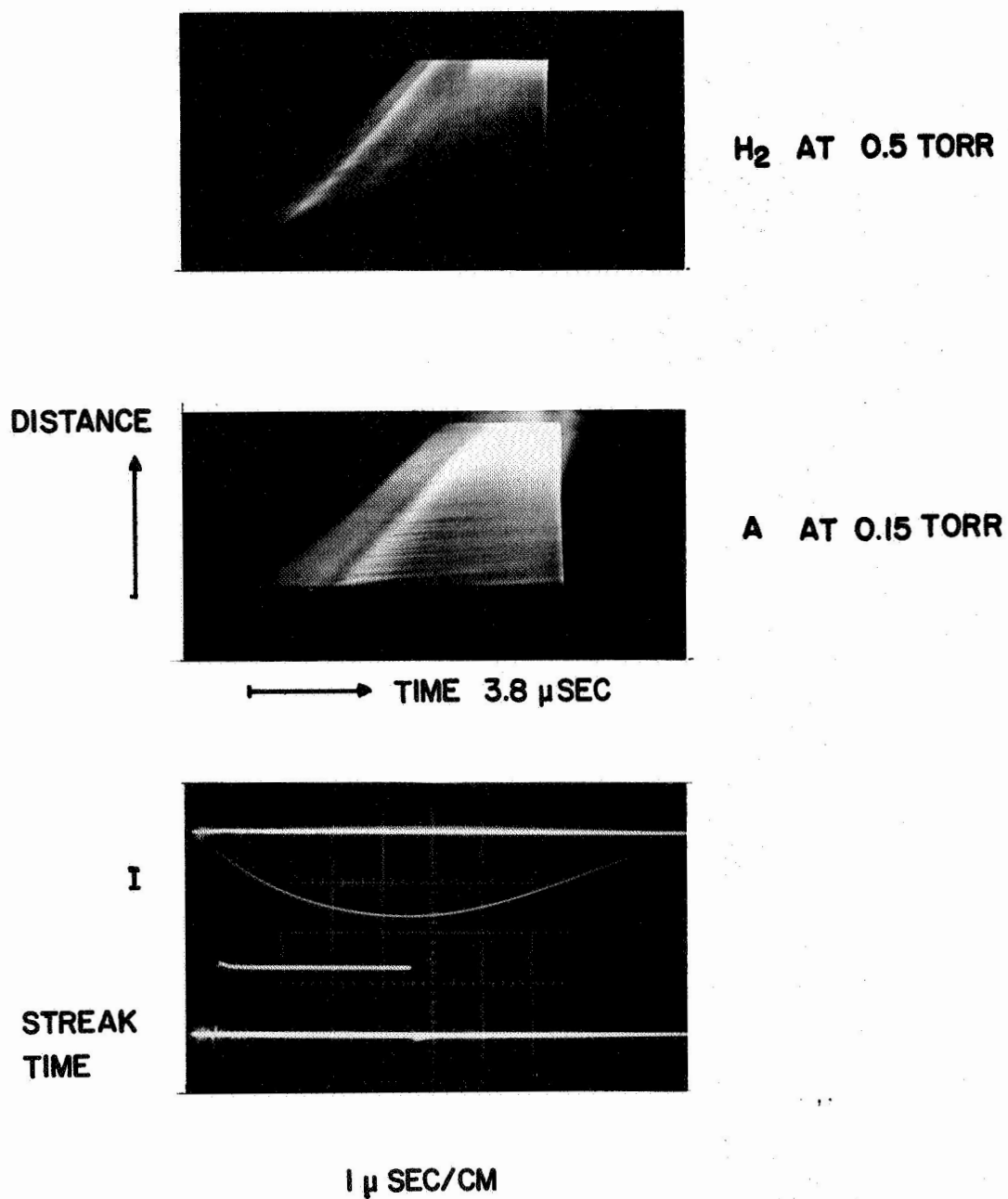
H₂ AT 0.5 TORR

DISTANCE

A AT 0.15 TORR

TIME 3.8 μSEC

I

STREAK
TIME

I μ SEC/CM

FIG. 1   STREAK PHOTOGRAPH OF LUMINOUS FRONT WITH SIMULTANEOUS
RECORDING OF DISCHARGE CURRENT AND STREAK MONITOR SIGNAL

6

non-refractory insulators has not been done to the best of our knowledge. In order to avoid further complications, the accelerator geometry is kept the same while the insulators are changed from one material to another for comparison. Four different insulator materials are used with accelerator # 7A and the sheet velocities are measured at fixed capacitor charging voltage. The result is shown in Fig. 2 where the measured velocities are plotted against the filling pressure of nitrogen. The velocities corresponding to the trials with insulator materials of lucite and mylar give approximately the same value in the pressure range used here. The velocities with vycor and pyrex glass are also very close to each other within the experimental scatter. However, one notices a large velocity difference between the two groups of insulators, i.e., velocities with a lucite insulator give about 65 per cent of that with vycor glass. Fig. 3 shows the similar measurement in hydrogen filling and again one finds that the velocities with lucite are about 70 per cent of that with vycor glass. It should also be noted that all curves regardless of the insulator material approximately follow the snowplow prediction $U \propto \frac{1}{\rho^{\frac{1}{4}}}$, where U and ρ are the measured velocity and the gas density, respectively. (See section III C).

C. Process of Insulator Wall Ablation

The velocity difference observed in the accelerator with refractory and non-refractory insulators should almost certainly be caused by the ablation from the insulator wall. Keck [2] has already predicted that the inertial drag of material ablated from the walls is the main source of the velocity limitation in an accelerator where non-refractory material is used. According to him, the ablation of the insulator wall takes place in the early stage of the discharge. The material from the wall quickly becomes ionized and, since it is at rest in a strong electric field,
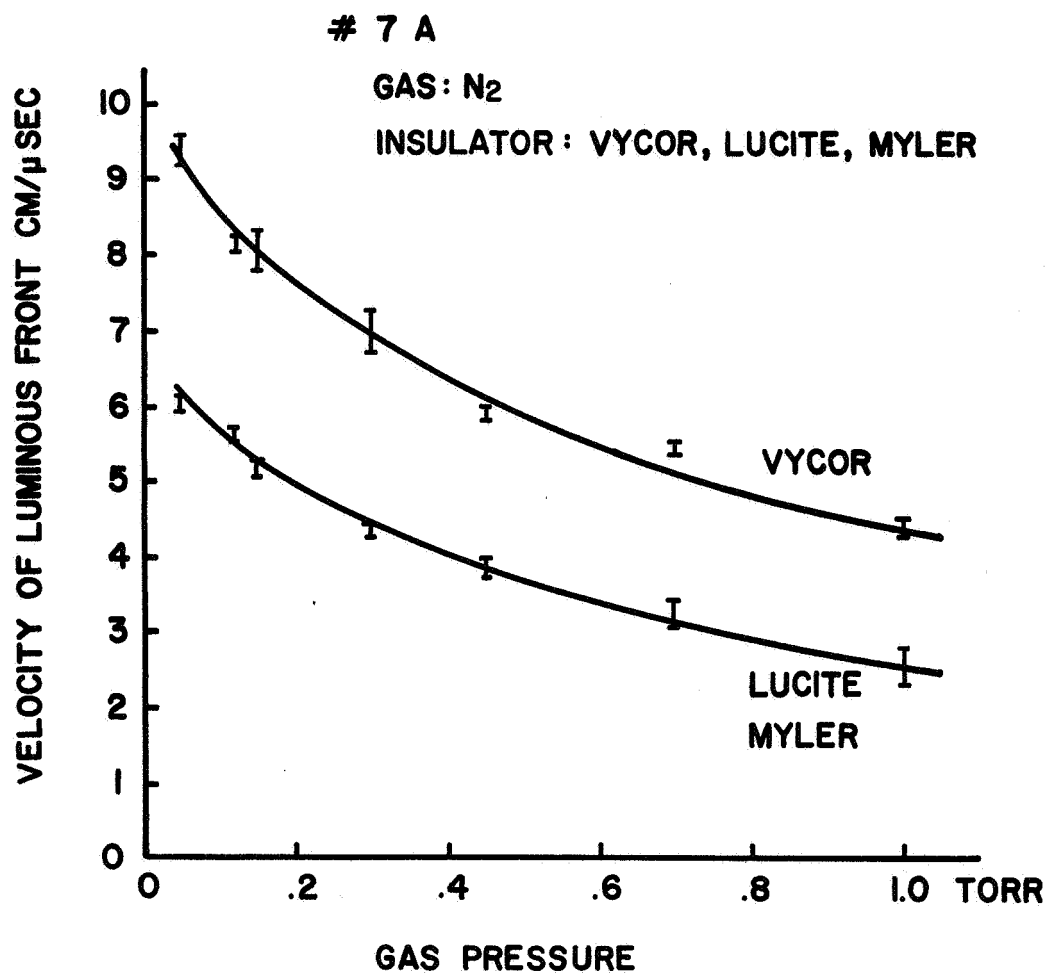
FIG. 2   COMPARISON OF VELOCITIES IN ACCELERATOR # 7A WITH REFRACTORY AND NON-REFRACTORY INSULATOR (N_2 GAS FILLING)
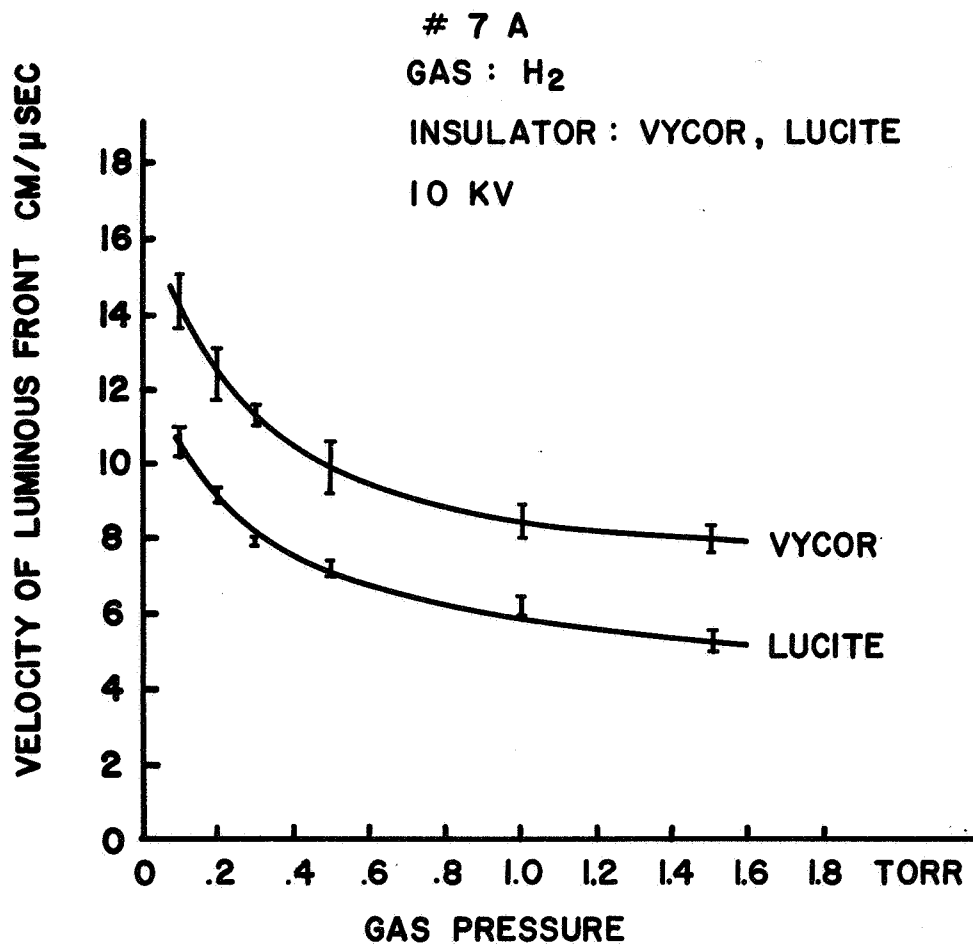
FIG. 3   COMPARISON OF VELOCITIES IN ACCELERATOR #7A WITH REFRACTORY
AND NON-REFRACTORY INSULATOR (H_2 GAS FILLING)

a current will flow producing both joule heating and acceleration of the material. A well-confined standing arc is formed close to the insulator wall and in turn transfers a portion of its heat (or energy) back to the insulator end-wall generating a continuous flow of vapor from the wall. Only a part of the total discharge current would flow in the current-sheet under this circumstance and this causes a reduction in the sheet velocity. The physical model[2] of the insulator ablation is illustrated in Fig. 4. The process is shown on a x - t diagram together with assumed profiles of the magnetic field B, the electric field E, the material velocity U and the current density J at a fixed time after the sheet speed has reached a steady value. The flow was divided into five regions: (1) initial test gas ahead to the current-sheet, (2) a thin region including the gas swept up by the current-sheet, (3) a region containing ablated material which grows with time but in which the ablated material is accelerated by a current at the wall and (5) a thermal boundary layer of thickness δ from which heat is conducted to the back wall to produce ablation.

A qualitative check on Keck's model is made experimentally. First, in order to examine the existence of ablated material flow behind the current-sheet, two monochromators are focused to two different axial locations of the accelerator barrel through the slots in the outer electrode. The line of sight of both monochromators is perpendicular to the accelerator axis. Among the probable impurities, the singly and doubly ionized carbon spectral lines seem to be the most intense lines behind the current-sheet when lucite is used as an insulator. Figure 5 (a) shows typical photoelectric signals of the CII 4267 $\overset{o}{A}$ line at $z = 7cm$ and $z = 15cm$ (insulator wall is $z = 0$) respectively. As can be seen the first arriving peak which has a relatively

10
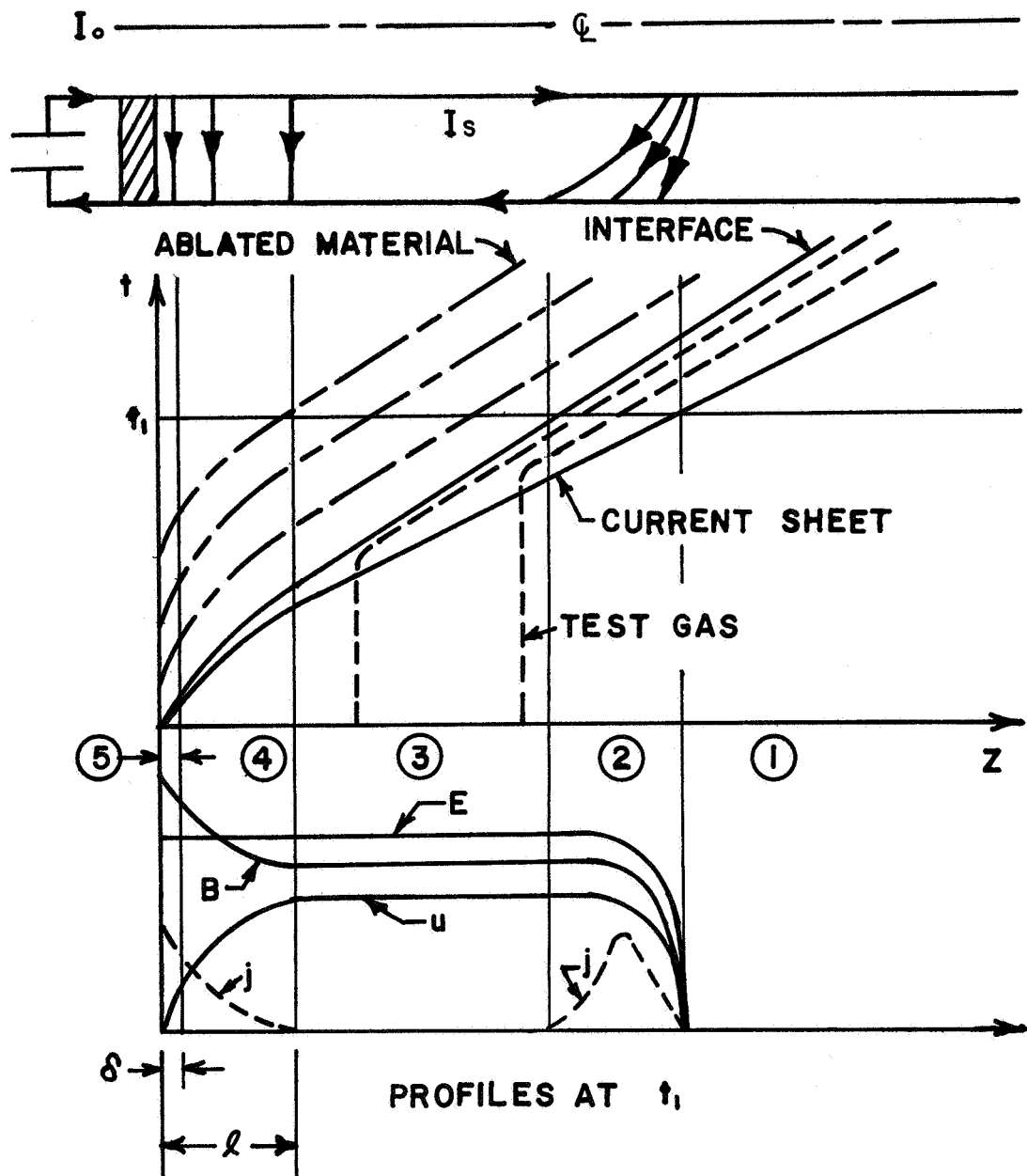
FIG. 4   x – t DIAGRAM SHOWING KECK'S MODEL OF INSULATOR WALL ABLATION (FROM REFERENCE 2)

(a)

Z = 7 CM

Z = 15 CM

CII 4267Å

10 KV

(b)

Z = 7 CM

Z = 15 CM

CII 4267Å

6 KV

2 μ SEC/DIV

H₂   AT I TORR

FIG. 5   (a) PHOTOELECTRIC SIGNALS OF CII 4267 Å AT z = 7 CM AND
                z = 15 CM (CHARGING VOLTAGE: 10 KV)
           (b) PHOTOELECTRIC SIGNALS OF CII 4267 Å AT z = 7 CM AND
                z = 15 CM (CHARGING VOLTAGE: 6 KV)

low amplitude is followed by a high and broad pulse. The initial carbon line signal coincides with the current-sheet and the second peak is the flow of ablated carbon atoms from the insulator. The propagation velocity of each pulse can be derived from the time delay measured on the oscillogram. Figure 5 (b) is a similar recording of the CII 4267 $\overset{o}{A}$ signal taken with a 6 KV charging voltage. The second peak in this case is very low in amplitude compared with the first peak in contrast with the 10 KV case. The third peak on the oscillogram is the current-sheet produced by a reversed discharge of second half-cycle. In order to check the carbon ion formation near the insulator wall, a monochromator is focused so as to look primarily at a portion of the volume in the vicinity of the insulator wall. This is done by observing the plasma from the back of the accelerato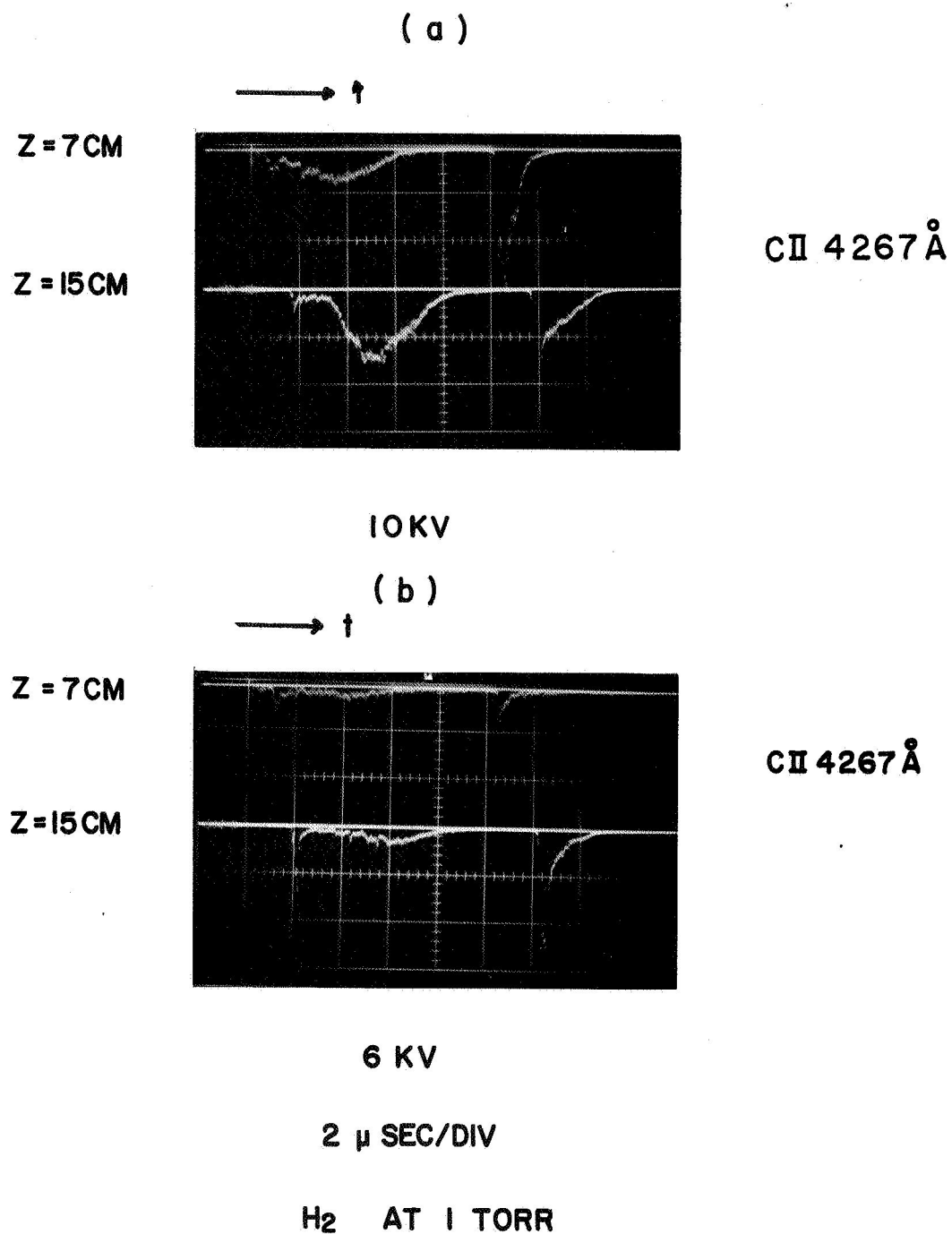r through the insulator disc. The photoelectric signals of the CII 4267 $\overset{o}{A}$ and CIII 4647 $\overset{o}{A}$ lines are shown in Fig. 6, where the discharge current waveforms are also recorded. The peaks of both CII and CIII line signals coincide with the discharge current maximum in time and the amplitude of the signal is negligibly small at the beginning and the end part of the first half cycle. This indicates that the ablation does not take place at the lower discharge current and this may be the reason why the second CII signal in the case of 6 KV in Fig. 5 (b) is so low in amplitude.

The same spectroscopic observations are made with Accelerator # 7A where vycor glass is used as an insulator. The carbon line signals appear to be far less intense than in the case of the lucite insulator and do not form a distinct second peak. Possible silicon lines are also examined but these line signals are found to be negligibly small. The above observations confirm that the carbon impurities are produced as a result of the insulator wall (lucite) ablation

CⅡ 4267Å

I
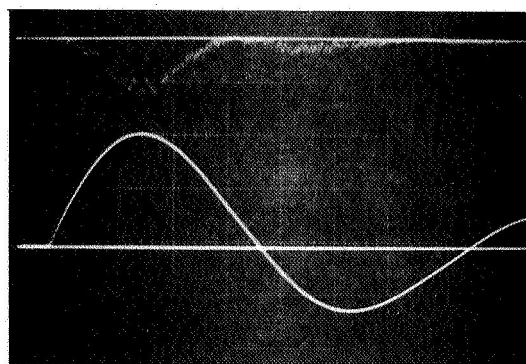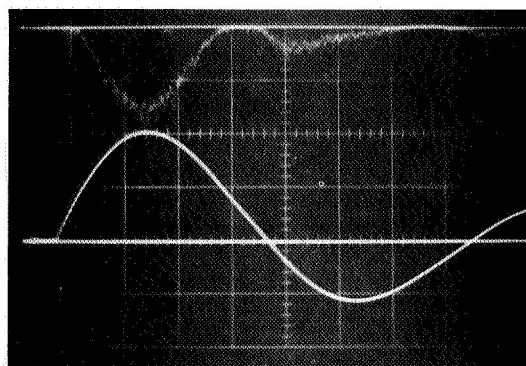
CⅢ 4647Å

I

2 µSEC/DIV

H₂   AT I TORR

FIG. 6   SIMULTANEOUS RECORDING OF DISCHARGE CURRENT AND
PHOTOELECTRIC SIGNALS OF CII 4267 Å AND CIII 4647 Å
OBSERVED IN THE VICINITY OF INSULATOR WALL

and that the current-sheet is followed by a flow of ablated material (carbon) which supports Keck's model.

A magnetic probe is used to measure B_θ in order to determine the proportion of current carried in the current-sheet. The integrated probe signals with Accelerator # 7A with lucite and vycor glass insulators are shown for comparison in Fig. 7. As can be seen the signal waveforms are different, i.e. the current carried in the current-sheet in the case of the lucite insulator is very small compared with the case of the vycor glass insulator. One also sees a considerable portion of the discharge current conducted in the region behind the current-sheet probably through the ablated material. Figure 8 shows the measured radial current in the annulus where results with two different capacitor charging voltage are compared. In the case of 10 KV, the current carried by the sheet is less than 50 per cent whereas about 80 per cent of the total discharg current is carried in the front with 6 KV. This is expected from the fact that far less ablation takes place with the low discharge current.

7A (Vycor Glass)

5 V/div

I

B_θ

7A (Lucite)

2 V/div

I

B_θ
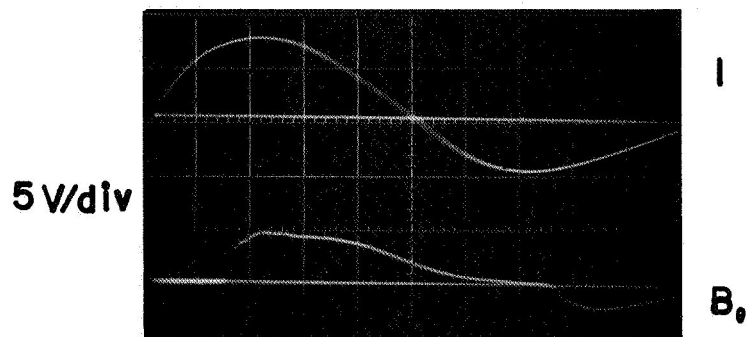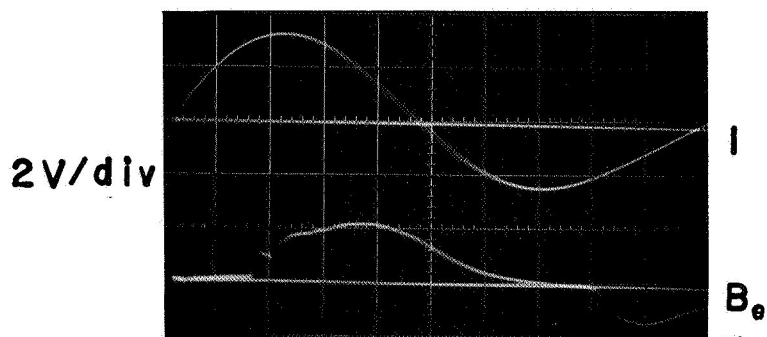
10 kV

2 μsec/div

H_2 at 1 torr

FIG. 7   COMPARISON OF MAGNETIC PROBE SIGNAL IN ACCELERATOR # 7A
WITH VYCOR GLASS AND LUCITE INSULATOR

FIG. 8   SKETCH OF DISCHARGE CURRENT AND INTEGRATED PROBE SIGNALS
COMPARING BETWEEN TWO DIFFERENT CHARGING VOLTAGES IN
ACCELERATOR # 7A (LUCITE)

III. Ablation Analysis

A. Workman's Analysis

Workman [6] has developed a theory about the insulator ablation which is based

on the physical model proposed by Keck. The conclusion of the analysis is that the ratio of
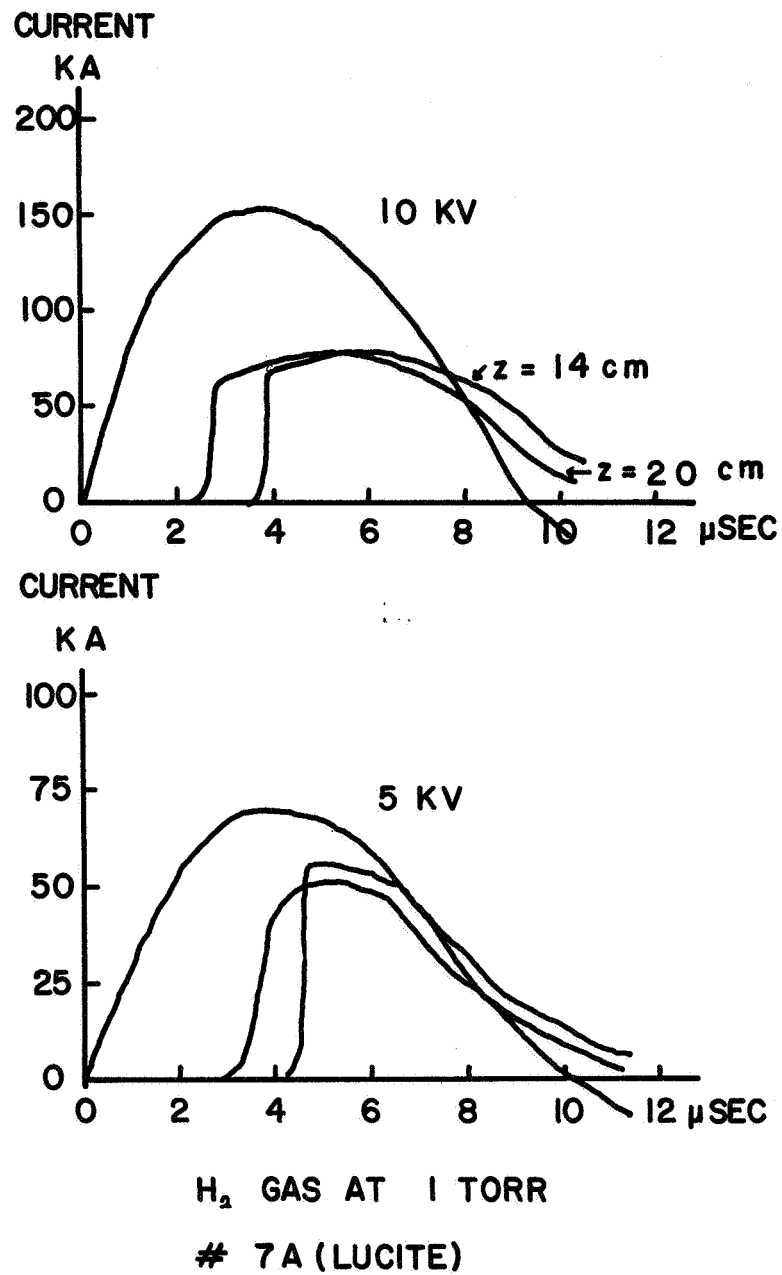
the observed velocity U_p to the ideal velocity U_o is determined solely by the correlation

parameter $\beta = \dfrac{2\epsilon_I}{m_A U_o^2}$, where ϵ_I and m_A are respectively the ionization potential

and atomic weight of the insulator material. The ideal velocity U_o is the velocity that

corresponds to the case of no ablation and is related to the magnetic field B_o and initial gas

density ρ by the expression [7] $\dfrac{B_o}{2\mu_o} = \dfrac{4}{3} \rho_g U_o^2$ where $B_o = \dfrac{\mu_o I_o}{2\pi r}$ and where I_o

and r are the total discharge current and the radius of the inner electrode, respectively. The

ratio $\dfrac{U_p}{U_o}$ decreases as U_o increases (or as β decreases) and the ratio falls rapidly for small

values of β.

Workman's result is examined experimentally under a wide variety of conditions of

accelerator operations. Figures 9 and 10 show a plot of $\dfrac{U_p}{U_o}$ vs. U_o for hydrogen and nitrogen

gas filling, respectively. The ideal velocity U_o is varied by changing the gas pressure, i.e,

ρ , while the charging voltage is kept at 10 KV. In general, the ratio $\left(\dfrac{U_p}{U_o} \right)$ drops rather

rapidly as the ideal velocity increases and the ratio is definitely higher with vycor glass than with

lucite insulator as expected. However, $\dfrac{U_p}{U_o}$ obtained in the accelerator with the vycor glass

(or pyrex) insulator, which is supposed to be a refractory material, also shows the very same

tendency as the lucite insulator indicating that the accelerator with refractory material may also

GAS: HYDROGEN

IO KV

7B (VYCOR)

#7A(VYCOR)

#7A(LUCITE)

$$U_o = \frac{B_o(r_i)}{(2\mu_o\rho)^{1/2}}$$

FIG. 9   PLOT OF $\frac{U_p}{U_o}$ VS. U_o FOR H_2 GAS FILLING

19

GAS : NITROGEN
IO KV

#7B (PYREX)

#7A(VYCOR)

#7C(LUCITE)

#7A(LUCITE)

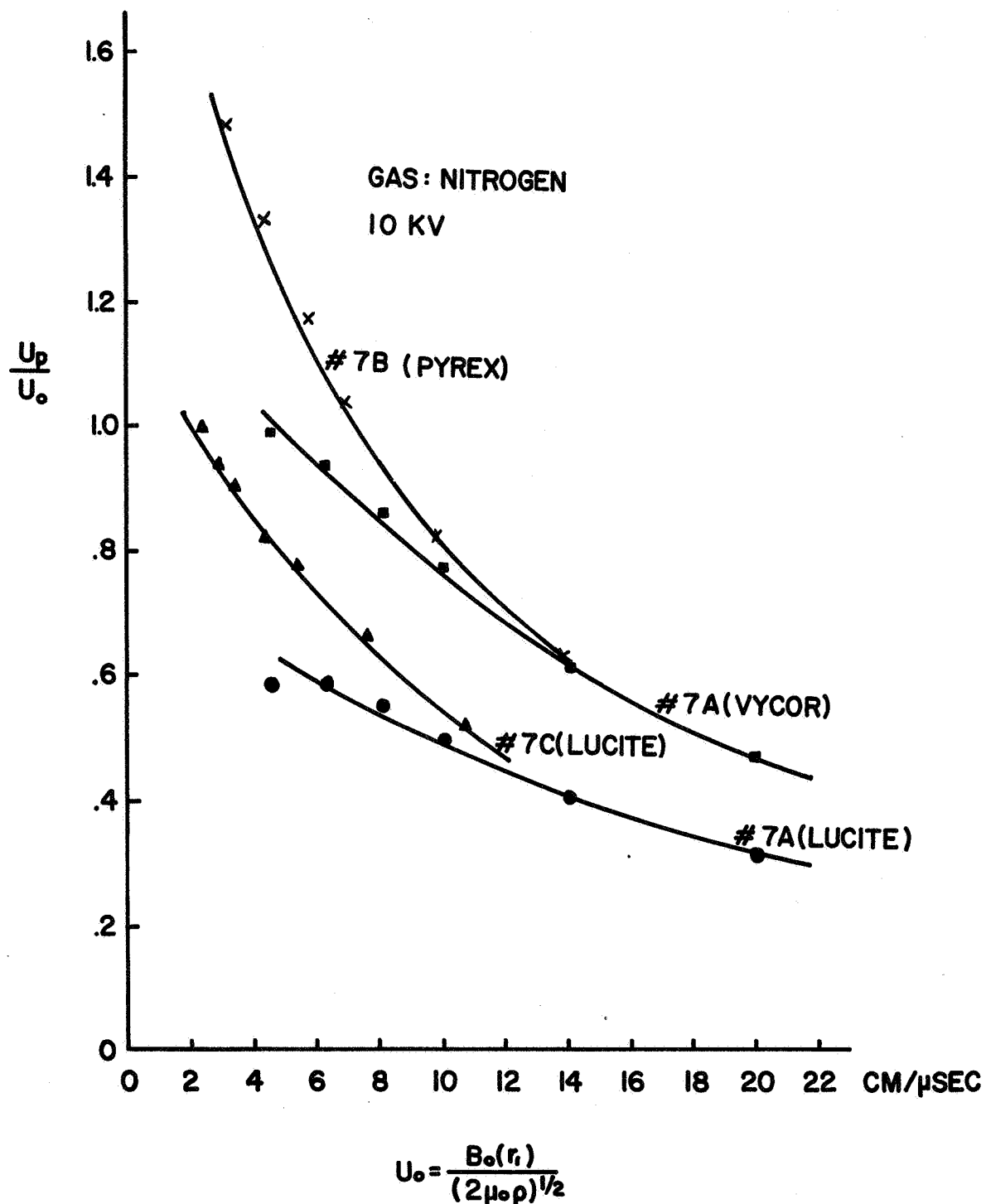$$U_o = \frac{B_o(r_i)}{(2\mu_o\rho)^{1/2}}$$
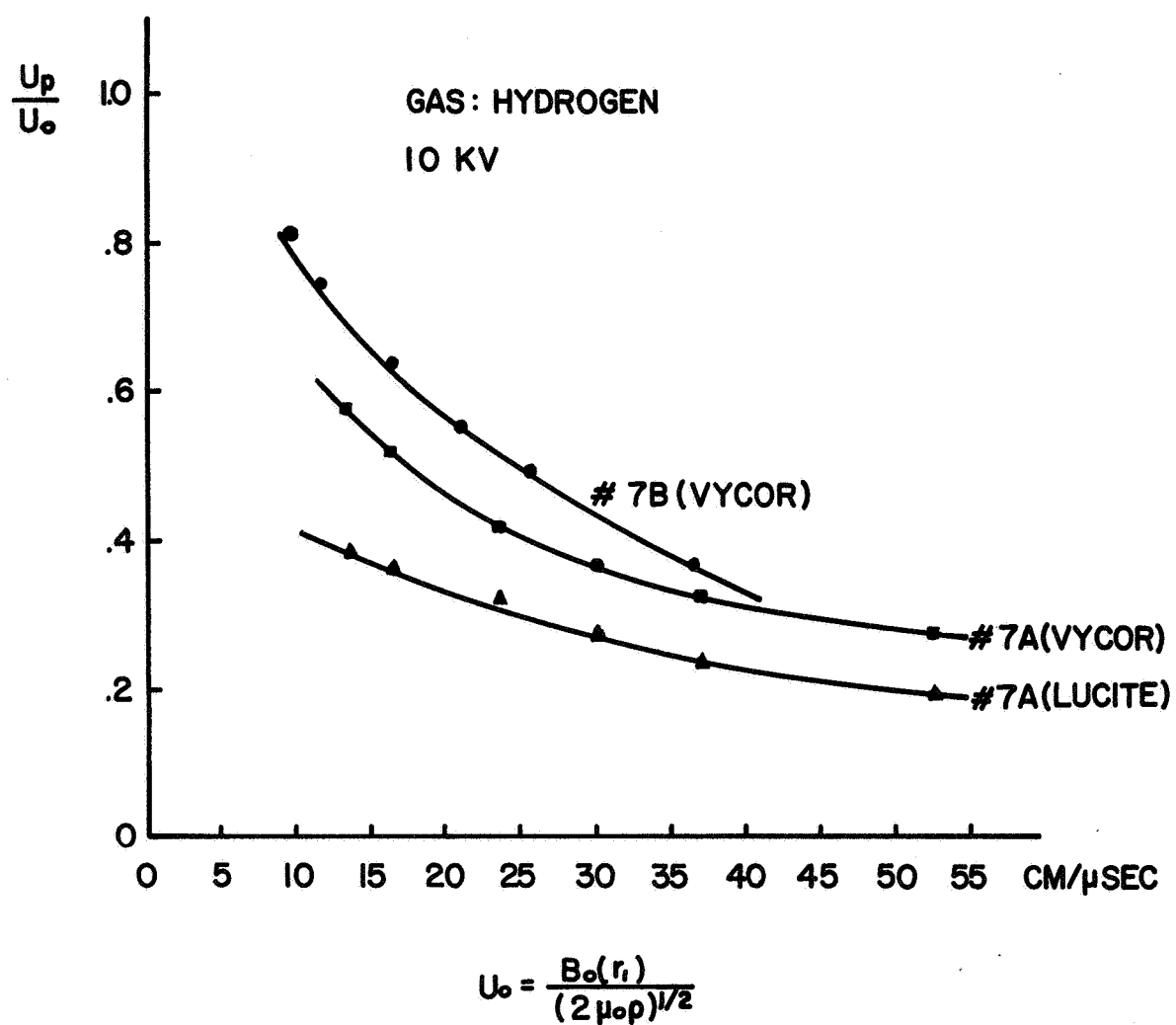
FIG. 10   PLOT OF $\frac{U_p}{U_o}$ VS. U_o FOR N_2 GAS FILLING

have a similar loss mechanism. The other important fact is that the ratio is also dependent on the accelerator geometry even with the same insulator material. This fact indicates that Workman's relation with a single correlation parameter does not hold generally. One notices that $\dfrac{U_p}{U_o}$ goes up beyond unity at lower value of U_o when nitrogen gas is used. This problem is discussed in section III C.

B. Analysis and Comparison with the Experiment

In Workman's treatment of the problem, he assumed the fraction of ionization in the vicinity of the insulator wall to be negligible. Spectroscopic signals shown in Fig. 6 indicate an abundant amount of singly and doubly ionized carbon atoms near the insulator wall while the current-sheet accelerates down the tube. Therefore, it is reasonable to assume that there is in fact a considerable fraction of ionization in this region. This assumption in turn brings in another correlation parameter which mostly depends on the accelerator geometry near the insulator and on the total discharge current.

We refer to Reference (6) for a description of the physical model for ablation originally proposed by Keck. Following Workman, we apply the conservation equations to the standing arc near the insulator end-wall. For the standing arc zone, the following quantities near the wall are denoted by the subscript "o" and those downstream by "d". Applying conservation of momentum and energy across the zone [6], one obtains

Momentum

$$n_{e_o} k\, T_e + \left(\frac{B_o^2}{2\mu_o} \right) = w\, U_d + \left(\frac{B_d^2}{2\mu_o} \right) , \qquad (1)$$

21

and

Energy

$$w \left(\frac{1}{2} U_d^2 + h_d \right) = E I \; , \tag{2}$$

where n_{eo} and T_e are the electron density and electron temperature near the

wall, respectively, w is the mass flow of ablated vapor,

B is the magnetic field,

h is the enthalpy,

E is the electric field,

and   I is the total current per unit width flowing in the arc.

We make use of the following relationships [6]

$$f = \frac{n_{eo}}{n_o} \; , \tag{3}$$

$$h_d = \frac{\epsilon_I}{m_A} \tag{4}$$

$$n_o = \frac{w}{m_A U_{th}} \tag{5}$$

$$U_{th} = \left(\frac{8 k T_w}{\pi m_A} \right)^{\frac{1}{2}} \tag{6}$$

$$E = U_d B_d \tag{7}$$

and $$I = \frac{B_o - B_d}{\mu_o} \tag{8}$$

where f is the fraction of gas ionized at the wall,

m_A is the atomic weight of the insulator material,

ϵ_I is the ionization potential of insulator material,

n_o is the gas number density near the wall,

and U_{th} is the initial velocity and is taken to be the termal velocity corresponding to the wall temperature T_w.

Using the above relationships, Eqs. (1) and (2) become

$$w\left[U_d - fk\left(\frac{\pi \, T_e^2}{T_w \, 8k \, m_A}\right)^{\frac{1}{2}}\right] = \frac{1}{2\mu_o}\left(B_o^2 - B_d^2\right), \qquad (9)$$

and $$w\left[\frac{\epsilon_I}{m_A} + \frac{1}{2}U_d^2\right] = \frac{U_d \, B_d}{\mu_o}\left(B_o - B_d\right), \qquad (10)$$

The above equations can be combined to yield

$$\frac{B_d}{B_o} = \frac{1 + \dfrac{2\epsilon_I}{m_A \, U_d^2}}{3 - \dfrac{2\epsilon_I}{m_A \, U_d^2} - \dfrac{4fk}{U_d}\left(\dfrac{\pi \, T_e}{8k \, m_A \, T_w}\right)^{\frac{1}{2}}}. \qquad (11)$$

Defining the dimensionless parameters

$$\alpha = \frac{2\epsilon_I}{m_A \, U_d^2}, \qquad (12)$$

and $$\nu = \frac{\pi f}{2}\frac{T_e}{T_w}\frac{U_{th}}{U_d}, \qquad (13)$$

Eq. (11) becomes

$$\frac{B_d}{B_o} = \frac{1 + \alpha}{3 - \alpha - \nu}. \qquad (14)$$

23

Denoting the flow quantities at the magnetic piston by the subscript "p", the magnetic field and velocity are related by

$$\frac{B_p^2}{2\mu_o} = \frac{4}{3} \rho_g U_p^2 \, ,$$ (15)

where ρ_g is the initial test gas density. From Eq. (15), an "ideal" velocity that corresponds to the no-ablation case can also be defined by

$$\frac{B_o^2}{2\mu_o} = \frac{4}{3} \rho_g U_o^2 \, .$$ (16)

It is convenient to introduce two new dimensionless parameters, i.e.,

$$\beta = \frac{2 \epsilon_I}{m_A U_o^2} = \left(\frac{U_d}{U_o}\right)^2 \alpha \, ,$$ (17)

and $$\eta = \frac{\pi f}{2} \frac{T_e}{T_w} \frac{U_{th}}{U_o} = \frac{U_d}{U_o} \nu \, .$$ (18)

Equation (14) becomes

$$\frac{B_d}{B_o} = \frac{1 + \dfrac{\beta}{(U_d/U_o)^2}}{3 - \dfrac{\beta}{(U_d/U_o)^2} - \dfrac{\eta}{(U_d/U_o)}} \, .$$ (19)

Since $\dfrac{B_d}{B_o} = \dfrac{U_d}{U_o}$, one obtains the following equation for $\dfrac{U_d}{U_o}$

$$3\left(\frac{U_d}{U_o}\right)^3 - (1 + \eta)\left(\frac{U_d}{U_o}\right)^2 - \beta\left(\frac{U_d}{U_c}\right) - \beta = 0 \, .$$ (20)

Note that if $\eta = 0$, one recovers eq. (18) of Reference (6). Thus the relative value of η compared to unity determines whether this parameter can be neglected.

Two types of solutions are considered following Reference (6) i.e., (1) the magnetic piston has a sub-Alfvén speed or (2) the piston velocity is super-Alfvénic. Let $ß = ß_c$ be a value of $ß$ which separates the two flow regimes and one can easily derive the following equation

$$\beta_c = 0.461 \left(\frac{U_d}{U_o}\right)_c^2 - \frac{\eta}{2.73} \left(\frac{U_d}{U_o}\right)_c , \tag{21}$$

where $\left(\frac{U_d}{U_o}\right)_c$ is determined from

$$\left(\frac{U_d}{U_o}\right)_c = \frac{1.461 - \frac{\eta}{2.73} + \sqrt{\left(1.461 - \frac{\eta}{2.73}\right)^2 - 3.73\eta}}{5.08} . \tag{22}$$

For $ß > ß_c$ the piston velocity is sub-Alfvénic and $U_p = U_d$. Putting $U_p = U_d$ into Eq. (20), one obtains

$$3\left(\frac{U_p}{U_o}\right)^3 - (1 + \eta)\left(\frac{U_p}{U_o}\right)^2 - \beta\left(\frac{U_p}{U_o}\right) - \beta = 0 \tag{23}$$

$$\beta_c \leq \beta \leq 1$$

of which the solution is

$$\frac{U_p}{U_o} = A^{\frac{1}{3}} + B^{\frac{1}{3}} + \frac{1+\eta}{9} \tag{24}$$

where

$$A = -\frac{q}{2} + \sqrt{\frac{q^2}{4} + \frac{p^3}{27}} \; ,$$

$$B = -\frac{q}{2} - \sqrt{\frac{q^2}{4} - \frac{p^3}{27}} \; ,$$

$$p = -\frac{(1+\eta)^2}{27} - \frac{\beta}{3} \; ,$$

$$q = -\frac{2}{3^6}(1+\eta)^3 - \frac{\beta(1+\eta)}{27} - \frac{\beta}{3} \; .$$

For $0 \le \beta \le \beta_c$ the velocity U_d and U_p are related by the following equation

$$U_p - U_d = 2\left(\frac{B_d U_d}{\mu_o w}\right)^{\frac{1}{2}}\left[(B_d)^{\frac{1}{2}} - (B_p)^{\frac{1}{2}}\right] \; . \tag{25}$$

Using this relation, we obtain a solution of Eq. (20) for the super-Alfvénic case, i.e.,

$$\left(\frac{U_p}{U_o}\right)\left(\frac{U_d}{U_o}\right)^{-1} = 3 - 2(3)^{\frac{1}{4}}\left(\frac{U_p}{U_o}\right)^{\frac{1}{2}} \; , \tag{26}$$

$$0 \le \beta \le \beta_c$$

where $\dfrac{U_d}{U_o}$ is given by

$$0.461\left(\frac{U_d}{U_o}\right)^2 - \frac{\eta}{2.73}\left(\frac{U_d}{U_o}\right) - \beta = 0$$

or

$$\left(\frac{U_d}{U_o}\right) = \frac{\frac{\eta}{2.73} + \sqrt{\frac{\eta^2}{(2.73)^2} + 1.84\beta}}{0.92} \; . \tag{27}$$

Equations (24) and (26) are plotted in Fig. 11 giving the ratio of the actual magnetic

piston velocity to the ideal velocity as a function of β and the parameter η . The case of

$\eta = 0$ corresponds to Workman's result. On the same graph, experimental values are also

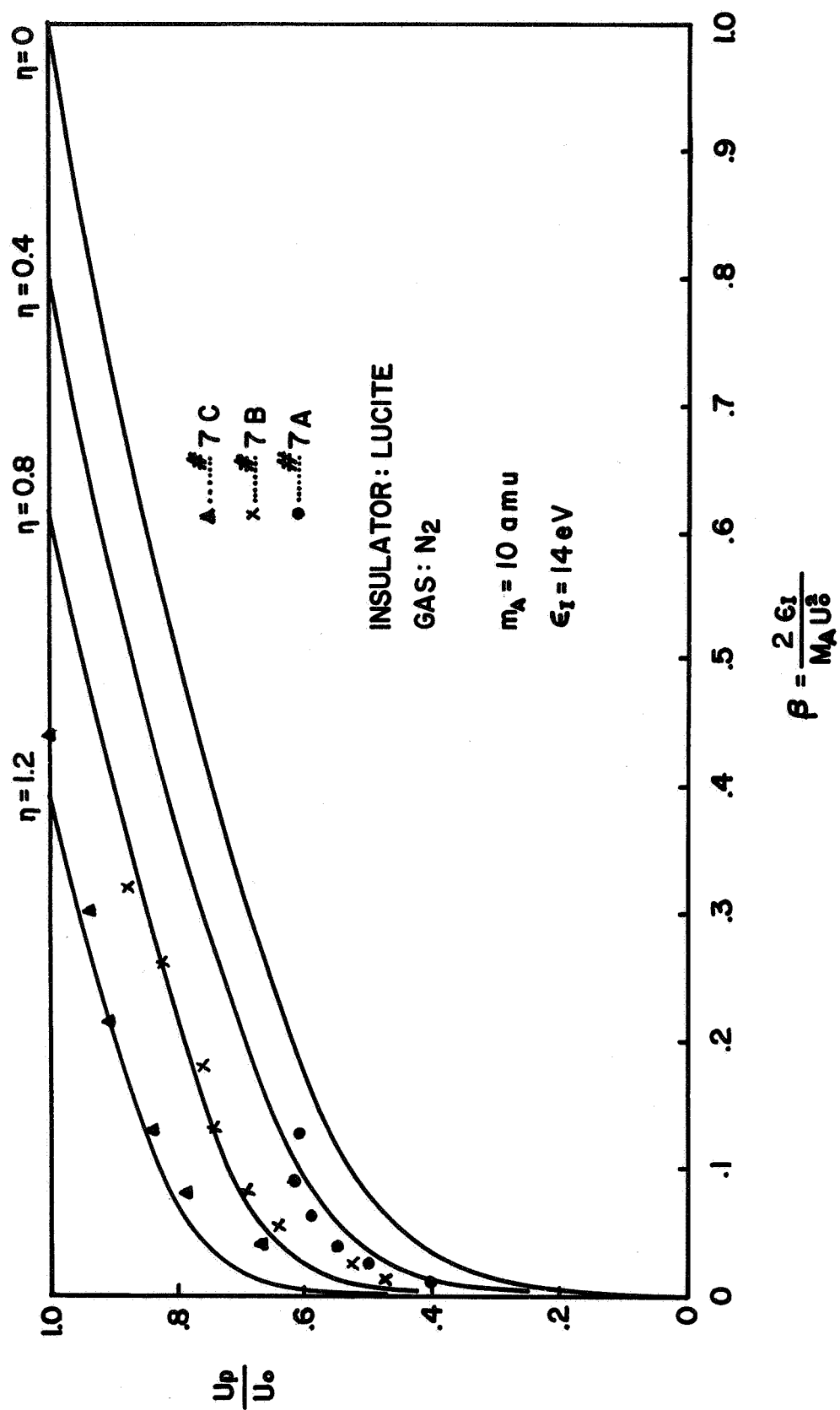FIG. 11   PLOT OF $\frac{U_p}{U_o}$ AS A FUNCTION OF $\left(\beta = \frac{2\epsilon_I}{m_A U_o^2} \right.$, (10 KV)

$\beta = \frac{2\epsilon_I}{M_A U_o^2}$

INSULATOR : LUCITE

GAS : N_2

$m_A = 10$ amu

$\epsilon_I = 14$ eV

▲......#7C
×......#7B
●......#7A

27

plotted for comparison. U_0 is varied by changing the gas pressure while the charging voltage

of the capacitor is kept at 10 KV. One immediately notices the ratio $\frac{U_p}{U_0}$ depends on the

accelerator geometry and is, not in agreement with Workman's result in these cases, i.e.,

$\eta = 0$. In general, the smaller the radius ratio $\frac{r_2}{r_1}$ is, the greater is the ratio $\frac{U_p}{U_0}$. Figure 12

shows the same plot of $\frac{U_p}{U_0}$ vs. ß for Accelerator #7B where two cases of different capacitor

charging voltage are compared. As can be seen, the $\eta = 0.8$ curve for 6KV and the $\eta = 1.2$

curve for 10 KV seem to fit approximately with the measured value. This difference can be

expected from the data shown in Fig. 5 (b). Experimental points of $\frac{U_p}{U_0}$ in the super-Alfvénic

regime of ß do not seem to fit well with the theoretical curve in both cases of Fig. 11 and

Fig. 12 and show more or less lower values of $\frac{U_p}{U_0}$.

Experimental evidence including Fig. 9 and 10 implies that in an accelerator with a

vycor (or pyrex) glass insulator and with a reasonably clean system, the velocity limitation of the

current-sheet is very much in the same manner as that for a non-refractory insulator. The

spectroscopic survey indicates far less intense carbon lines near the insulator wall of vycor glass

than that of lucite or mylar; however, some other material other than glass itself may be degassed

from it causing a loss similar to the wall ablation. In fact this process of degassing is

indistinguishable from the wall vaporization in the above analysis. It is known [8] that quartz,

vycor and pyrex glass are capable of absorbing extraordinary amounts of light gases such as helium

and hydrogen within a short period of time. Therefore, it is quite conceivable that a considerable

amount of hydrogen is degassed from the insulator wall during the discharge and immediately ionized

to form a standing arc. The ratio $\frac{U_p}{U_0}$ is plotted against ß with Accelerator #7A which uses

28

FIG. 12   PLOT OF $\frac{U_P}{U_o}$ AS A FUNCTION OF $\beta = \frac{2\,\epsilon_I}{m_A\,U_o^2}$
(10 KV AND 6 KV)

$\beta = \frac{2\,\epsilon_I}{m_A\,U_o^2}$

$\frac{U_P}{U_o}$

η = 0.8

η = 1.2

7B (LUCITE)

GAS: N₂

● · · · · 6 KV

x · · · · 10 KV

$m_A = 10$ amu

$\epsilon_I = 14$ eV

29
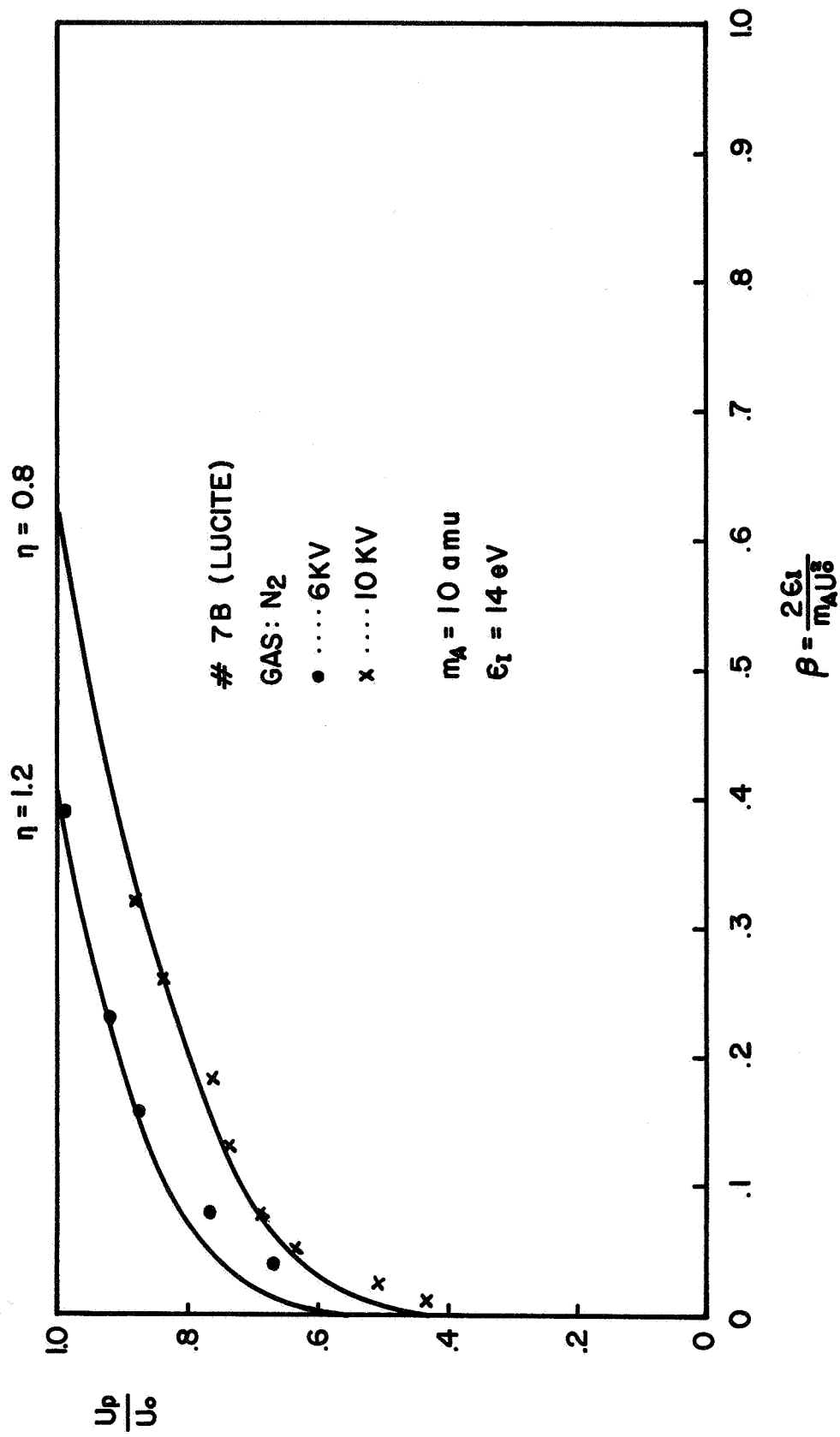
vycor glass as an insulator. Taking $m_A = 1$ (hydrogen) instead of $m_A = 10$ one obtains the result shown in Fig. 13 and experimental points fit well with the curve of $\eta = 0$. The current sheet velocity with vycor insulator is higher than that with the lucite insulator in the same accelerator geometry and at the same filling pressure because of its lighter atomic weight of exhausted gas from the former insulator; however, it still has the same loss mechanism and its current-sheet velocity is severely limited at a higher value of U_o. The absorption and the desorption of the gas from the vycor insulator may be reduced somewhat by repeating the discharge and evacuation(discharge cleaning)but it may be difficult to eliminate the absorption since it has a good chance of absorbing hydrogen gas again right after the discharge, during the gas flushing and refilling time. The quantity of hydrogen released by the insulator, electrodes, etc., during the discharge may not be small even in a reasonably clean system.

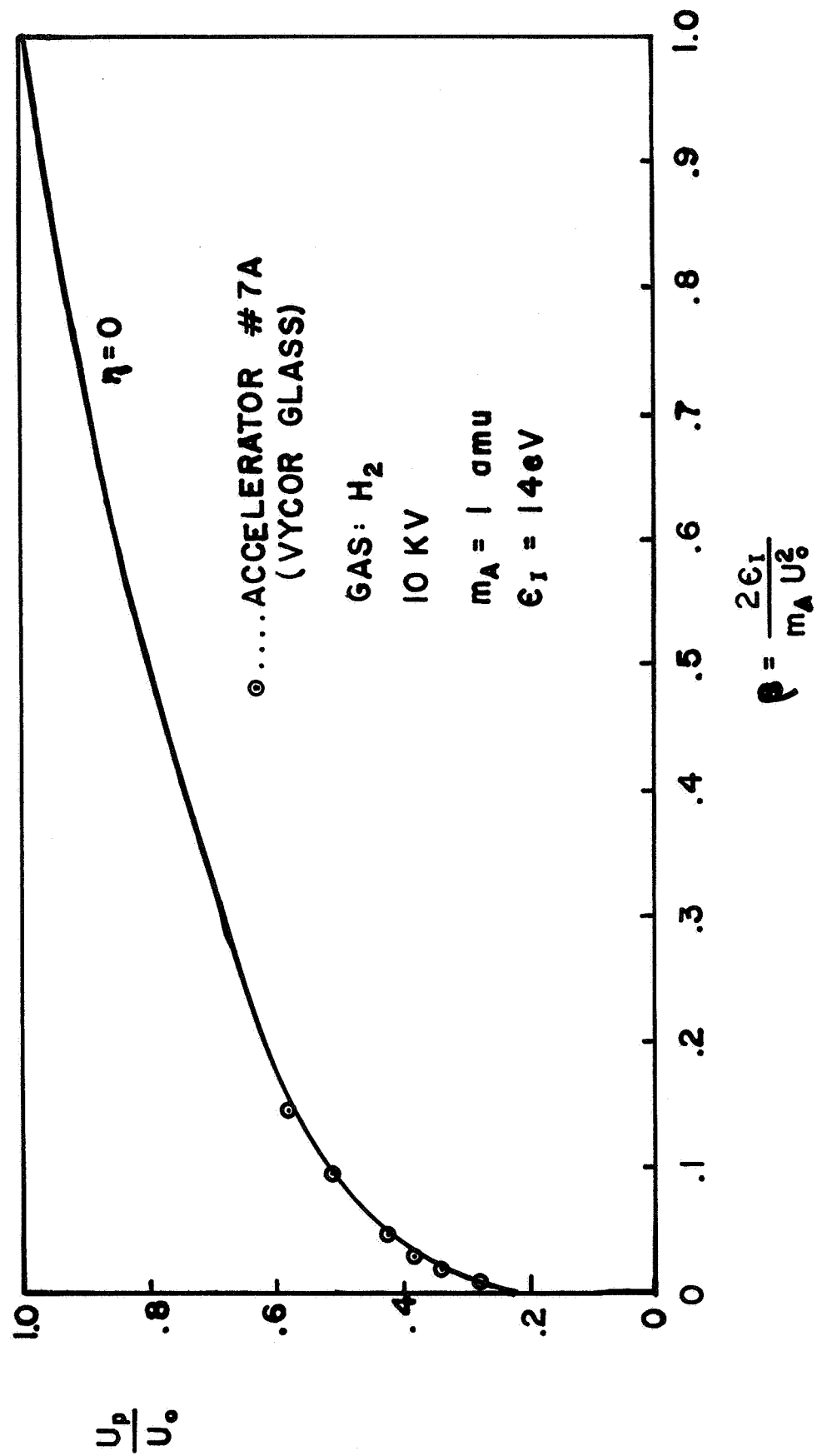FIG. 13   PLOT OF $\frac{U_p}{U_o}$ AS A FUNCTION OF β FOR #7A (VYCOR GLASS)

$\eta = 0$

$\circledcirc$ .... ACCELERATOR #7A
(VYCOR GLASS)

GAS: H_2

IO KV

$m_A = 1$ amu
$\epsilon_I = 14 eV$

$\beta = \dfrac{2\epsilon_I}{m_A U_o^2}$

$\dfrac{U_p}{U_o}$

B. Miscellaneous Remarks

The value of $\frac{U_p}{U_o}$ for Accelerator $\#$ 7C and 7B is higher than for Accelerator $\#$ 7A.

This is due to the fact that the sheet velocity measured with Accelerator $\#$ 7B and 7C is higher

for their radius ratio compared with that observed in Accelerator $\#$ 7A. According to the

relation of $U_p = \frac{B_\theta(r_i)}{(2\mu_o \rho)^{\frac{1}{2}}}$, velocities of the leading front with Accelerator $\#$ 7B (r = 16 mm)

and $\#$ 7C (r = 20 mm) should be about 70 per cent and 55 per cent of that with Accelerator $\#$ 7A

(r = 11 mm) respectively. Fig. 14 and 15 show a large departure from the above prediction and

the analysis described in a previous section assumes this is due to the difference in insulator

wall ablation or similar loss (degassing) among accelerators of different geometry. However,

as to whether the discrepancy is solely due to the ablation loss has yet to be confirmed.

Furthermore, an accelerator with a larger inner electrode diameter, i.e. $\#$ 7C and

7B, tend to give $\frac{U_p}{U_o}$ greater than unity at a lower value of U_o ($U_o <$ 7 cm/μsec) in nitrogen

and argon gas when a refractory material is used as an insulator (Fig. 10). This means the

measured velocities are greater than the ideal velocity of $U_o = \frac{B_\theta(r_i)}{(2\mu_o \rho)^{\frac{1}{2}}}$ where B_o $(r_1) = \frac{\mu_o I_o}{2\pi r_i}$

and I_o is the total discharge current. This may be an indication that some other

mechanism of plasma acceleration exists in this range of sheet velocity.

The current-sheet velocities in hydrogen, nitrogen and argon gas filling are plotted

against gas density and a log-log plot of this is shown in Fig. 16. As stated earlier, one can

see the measured values in hydrogen and argon fall well into lines which have slope of $\rho^{-\frac{1}{4}}$,

and are in agreement with the snowplow model in this range of gas density. However, one notices

that in the case of argon, the velocity is higher than in the case of hydrogen.
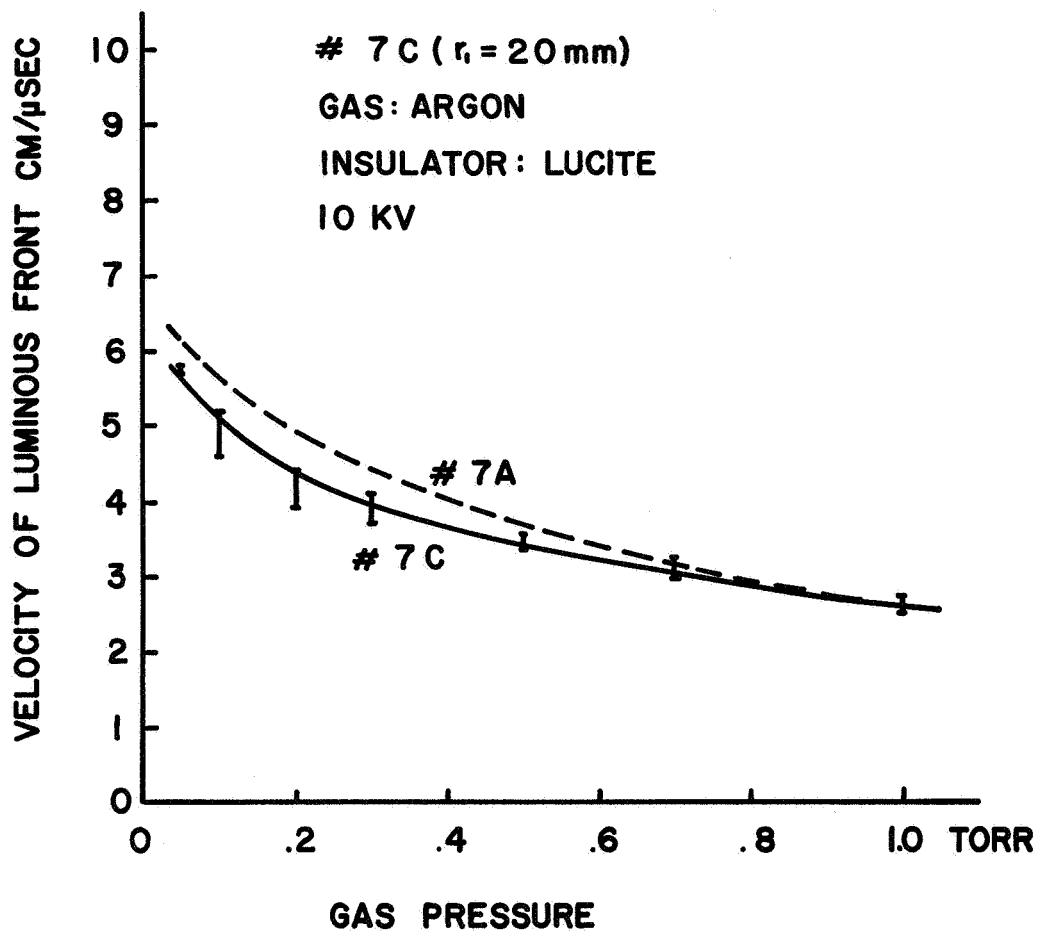
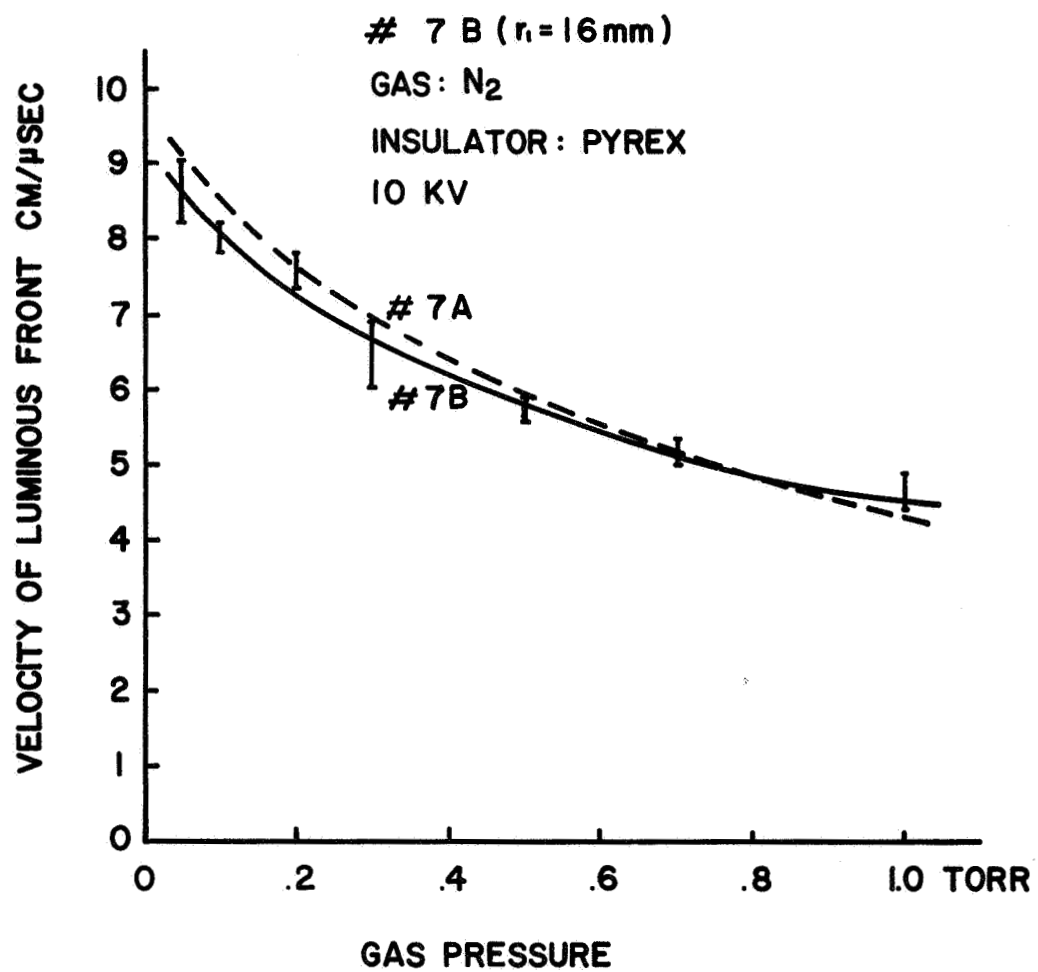FIG. 14   COMPARISON OF VELOCITIES IN ACCELERATOR # 7A AND # 7C

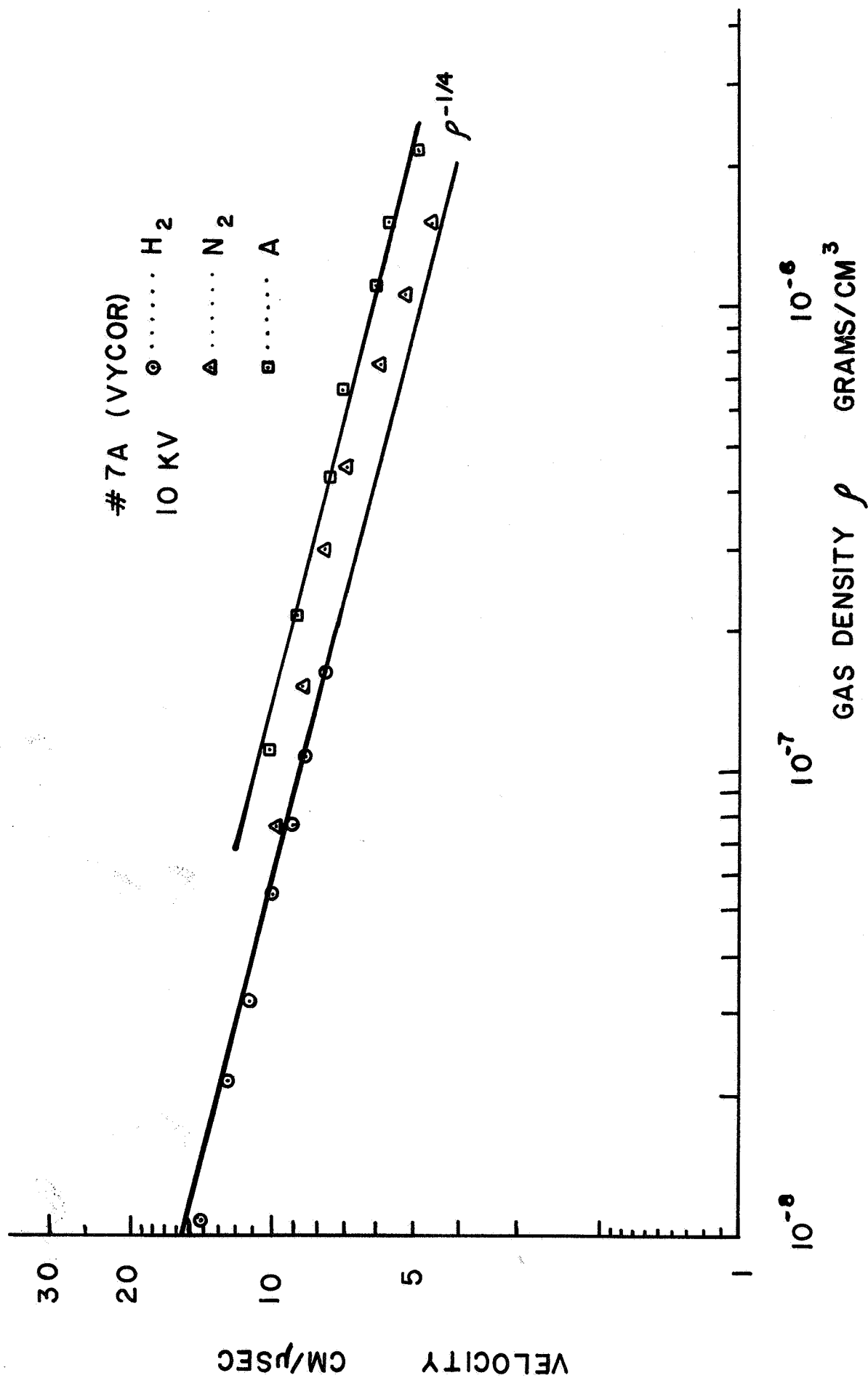FIG. 15   COMPARISON OF VELOCITIES IN ACCELERATOR # 7A AND # 7B

FIG. 16   VELOCITY AS A FUNCTION OF DENSITY OF FILLING GAS

35

IV. Conclusion

The current-sheet velocities in the two groups of coaxial plasma accelerators where refractory and non-refractory materials are used as an insulating disc, respectively, are compared in a wide variety of operating conditions. There exists a large difference in sheet velocity between the two groups of accelerators in all cases, i.e., the velocities in the accelerators with non-refractory insulators are slower than the others. A direct cause for this is that the measured radial current in the current-sheet is very small (being only a fraction of the total discharge current) compared to the accelerators with a refractory insulator. The impurity mass flow (mainly carbon atoms) which follows the accelerating current-sheet is observed and the impurity flow is mainly produced as a result of the insulator (non-refractory) wall ablation. The experimental observations appear to generally support Keck's proposed model of the ablation loss mechanism. The accelerators with vycor (or pyrex) glass and with reasonably clean system also have a severe loss process at a higher sheet velocity. In this case probably degassing of hydrogen (or helium) from the insulator is responsible for the drag rather than ablation. An analysis of the ablation problem is made mainly following Workman's result but an additional dimensionless parameter η is included. The parameter η enters as a result of an assumption that the fraction of the ionization in the vicinity of the insulator wall is not negligible and this is found to account for the geometric effect of an accelerator on the ratio $\dfrac{U_p}{U_0}$. The analytical curves which plot $\dfrac{U_p}{U_0}$ vs. β seem to fit reasonably well with the measurements except for the very low values of β (super Alfvénic regime). The plot of the sheet velocity vs. gas density show typical snowplow-type dependence of the gas density regardless of its insulator material or species of filling gas in the gas pressure range used in this investigation.

Acknowledgement

The authors wish to acknowledge the assistance given by Jack Williams and M.J. Rhee,

graduate assistants and also advices given by Mr. E.A. McLean and Dr. R.C. Elton of

the Naval Research Laboratory, Washington, D.C.

REFERENCES

1.   K. Thom, J. Norwood, and N. Jalufka, Phys. Fluids 7, S67 (1964).

2.   J. Keck, Phys. Fluids 7, S16 (1964).

3.   J.W. Mather and A.H. Williams, Rev. Sci. Instr. 3, 297 (1960).

4.   T.N. Lie, A.W. Ali, E.A. McLean and A.C. Kolb, Phys. Fluids 10, 1545 (1967).

5.   T.N. Lie, A.W. Ali, E.A. McLean and C.C. Chang, 2nd Semiannual Progress Report, NASA NGR-09-005-025, Department of Space Science and Applied Physics, Catholic University of America (1967).

6.   J.B. Workman, Phys. Fluids 8, 2162 (1965).

7.   N.H. Kemp and H.E. Petchek, Phys. Fluids 2, 599 (1959).

8.   J.H. Leck, "Advances in Mass Spectrometry", Pergamon Press, Inc., New York, (1959).

PROJECT REFERENCES

1. "Diagnostics of Accelerating Plasma" Research Proposal for NASA Research Grant NGR-09-005-025, Feb. 1965.

2. "Spectroscopic Study of a Coaxial Plasma Gun", Bulletin 10 523, American Physical Society Meeting in Washington, D.C. April 26-29, 1965.

3. "Diagnostics of Accelerating Plasma" Part V, 102, Fifth NASA Intercenter Conference on Plasma Physics in Washington, D.C., May 24-26, 1966.

4. "First Semi-Annual Progress Report for the period March 1 - Aug. 31, 1966, Research Grant NGR-09-005-025. Report No. 66-010, Department of Space Science & Applied Physics, Catholic University of America, Washington, D.C.

5. "Electric Polarity Effect in Coaxial Plasma Accelerator", Paper 7C-1, Eighth Annual Meeting on Plasma Physics of American Physical Society, Boston Nov. 2-5, 1966.

6. "Plasma State in Coaxial Accelerator", Physics of Fluids 10 1545, 1967.

7. Second Semi-Annual Progress Report for the period September 1, 1966 - Feb. 28, 1967, Research Grant NGR-09-005-025, Report No. 66-021, Department of Space Science and Applied Physics, Catholic University of America, Washington, D.C.

8. "Magnetohydrodynamic Shock Wave Structure" by C.K. Liu, (Ph.D. Thesis 1967), Report No. 67-028, Department of Space Science and Applied Physics, Catholic University of America, Washington, D.C.

9. "Studies of Current-Sheet in a Coaxial Plasma Accelerator" paper No. 67-658, AIAA Electric Propulsion and Plasmadynamics Conference, Colorado Springs, Sept. 11-13 1967.

10. "Pre-ionization Phenomena in Pulsed Plasma Accelerator" paper E5, Proc. APS Topical Conference on Pulsed High-Density Plasmas, Los Alamos, Sept. 19-22, 1967.

11. 3 rd Semi-Annual Progress Report for the period March 1, 1967 - August 31, 1967, Research Grant NGR-09-005-025, Report No. 67-029, Department of Space Science and Applied Physics, Catholic University of America, Washington, D.C.